Research Square

Preprints are preliminary reports that have not undergone peer review.
They should not be considered conclusive, used to inform clinical practice,
or referenced by the media as validated information.

# Collagen-inspired biomimetic peptides as therapeutic agents against methylglyoxal-mediated damage

**Erik Suuronen**

esuuronen@ottawaheart.ca

University of Ottawa Heart Institute

**Sergio Garcia Schejtman**

University of Ottawa Heart Institute & University of Ottawa https://orcid.org/0000-0003-1908-7348

**Juan Figueroa Alegria**

University of Ottawa Heart Institute https://orcid.org/0009-0000-3920-4412

**Ramis Ileri**

University of Ottawa Heart Institute https://orcid.org/0000-0001-8128-118X

**Micaela Giannetti**

University of Ottawa Heart Institute https://orcid.org/0000-0001-5203-995X

**Jessica Hernandez Juarez**

University of Ottawa Heart Institute

**Bryan Liu**

University of Ottawa Heart Institute & University of Ottawa

**Emilio Alarcon**

University of Ottawa https://orcid.org/0000-0001-5100-6179

**Article**

**Keywords:**

**Posted Date:** April 30th, 2026

**DOI:** https://doi.org/10.21203/rs.3.rs-9509976/v1

**License:** This work is licensed under a Creative Commons Attribution 4.0 International License.
Read Full License

**Additional Declarations: Yes** there is potential Competing Interest. S.D.G.S., J.D.F.A., R.I., M.G., J.H.J., E.I.A., E.J.S. are listed as inventors in a patent application for the peptide technology presented herein.

Patent applicant: Ottawa Heart Institute Research Corporation, 40 Ruskin Street H2406 Ottawa, Ontario K1Y 4W7, Canada. Name of inventors: Sergio D. Garcia Schejtman, Juan D. Figueroa Alegria, Ramis Ileri, Micaela Giannetti, Jessica Hernandez Juarez, Emilio I. Alarcon, Erik J. Suuronen. Application number: US 63/935,135. Status of the application: filed on 12/09/2025. The specific aspect of manuscript covered in the patent application: Composition of matter for the collagen-like peptides, and the use of the collagen-like peptides as a methylglyoxal-trapping therapeutic agent.

# Collagen-inspired biomimetic peptides as therapeutic agents against methylglyoxal-mediated damage

Sergio D. Garcia Schejtman[1†], Juan D. Figueroa Alegria[1†], Ramis Ileri[1,2†], Micaela Giannetti[1], Jessica Hernandez Juarez[1,2], Bryan Liu[1], Emilio I. Alarcon[1,2,3*], and Erik J. Suuronen[1,2,4*]

[1] Bioengineering and Therapeutic Solutions (BEaTS) Research, Division of Cardiac Surgery, University of Ottawa Heart Institute, 40 Ruskin Street, Ottawa, Ontario, Canada, K1Y 4W7.

[2] Ottawa-Carleton Institute for Biomedical Engineering, University of Ottawa, 800 King Edward Avenue, Ottawa, Ontario, Canada, K1N 6N5.

[3] Department of Biochemistry, Microbiology, and Immunology, University of Ottawa, Ottawa, Ontario, Canada, K1H 8M5.

[4] Department of Cellular and Molecular Medicine, University of Ottawa, Ottawa, Ontario, Canada, K1H 8M5.

[†] These authors contributed equally.

Correspondence: ealarcon@uottawa.ca; esuuronen@ottawaheart.ca

**Abstract**

Damage from increased levels of advanced glycation end-products (AGEs) is linked to aging and health problems such as diabetes, neurological disorders, and cardiovascular disease. Methylglyoxal (MG), a primary AGE precursor, is metabolized under normal conditions by the enzyme glyoxalase-1 (Glo1). However, in aging and disease, conditions including hypoxia, inflammation, ischemia, and oxidative stress increase MG production while limiting Glo1 activity, leading to AGE accumulation. This suggests that MG may be a therapeutic target for limiting the damage caused by AGEs. In this work, short collagen-based peptide sequences with varying numbers and positions of the amino acid arginine (a target for MG) are generated, characterized, and tested for their ability to trap MG. The peptide with 3 arginine residues on the C-terminal forms the most stable triple helix structure and exhibits the best MG-trapping capacity. Endothelial cells cultured in the presence of MG and treated with the best peptide candidate have superior viability, express less RAGE (receptor for AGEs), and have decreased intracellular AGE accumulation compared to untreated cells. This peptide may be a promising therapeutic approach to trap MG and limit its negative effects on aging and disease.

## Introduction

Protein glycation is a non-enzymatic post-translational modification associated with aging and several diseases.[1, 2] It is a spontaneous reaction between amino or guanidino groups (mainly from lysine and arginine residues) in proteins with the carbonyl group of a reducing sugar. This process leads to various modified derivatives, also known as advanced glycation end-products (AGEs). The accumulation of AGEs has been linked with chronic inflammatory diseases,[3] diabetes,[4, 5] and neurological[6, 7] and cardiovascular diseases.[8, 9] Methylglyoxal (MG), a highly reactive dicarbonyl compound formed mainly as a by-product of glycolysis, is the primary precursor for AGEs,[10] and is increasingly being recognized as a major contributor to the pathology of many diseases.[11-13] In normal physiological conditions, MG is metabolized primarily by the enzyme glyoxalase-1 (Glo1). However, under pathological conditions, hypoxia, inflammation, ischemia, and oxidative stress can increase MG production while limiting Glo1 activity, leading to MG-derived AGE (MG-AGE) accumulation with MG-derived hydroimidazolone (MG-H1) being the main product formed, accounting for ~90% of all adducts.[14-17] While MG can promote inflammation and cell damage directly,[18-21] its AGEs can also trigger pro-inflammatory and oxidative processes by binding to the receptor for AGE (RAGE) on the surface of cells.[22, 23]

Based on this, MG is identified as a promising target for developing new therapies to reduce inflammation, oxidative stress, and cell/tissue dysfunction in aging and disease. One of the primary targets for MG glycation is the collagen present in the extracellular matrix (ECM) of tissues.[24, 25] Thus, ECM-mimicking biomaterial therapies (particularly those based on collagen) that can remove MG from the environment constitute an attractive approach to protect cells and tissues. Our team previously demonstrated that a collagen type I hydrogel injected at the epicardial surface of the infarcted mouse heart can "soak up" MG,[26, 27] which accumulates in the myocardium after MI.[28] This treatment reduced the presence of MG-H1 in the underlying myocardium, leading to less oxidative stress and improved contractility and cardiac function.[26] However, such materials that use natural polymers can be complex,[29] and recombinant proteins required for clinical use are expensive and difficult to manufacture. To address these issues, developing peptide therapeutics to treat disease is a rapidly growing research area. Some advantages of the peptide approach are lower production costs, customizable amino acid sequences and peptide function, reduced immunogenicity, and a smaller size that provides many delivery options.[30, 31] For example, to target MG, Sasaki et al. designed a dipeptide with a specific MG-scavenger moiety and demonstrated its

ability to inhibit protein glycation *in vitro*.[32] More recently, cyclic arginine-based short peptides with MG scavenging capacity were shown to reduce the glycation of serum albumin and MG-induced pain in mice.[33] While promising, a potential limitation is that such peptides are short and lack the stability conferred by a secondary or tertiary structure that would extend their half-life and prevent their rapid elimination *in vivo*.[30, 34]

Thus, an attractive approach for an MG-trapping peptide therapeutic would be one based on collagen designed with a 3D structure, reactivity, and stoichiometry for trapping reactive MG molecules. To this end, synthetic peptides of <50 amino acids offer several advantages, including their ability to mimic several biological functions of the full-length structure, their potential for self-assembly, the availability of functional groups for further chemical modification, and their cost-effective scale-up for clinical use.[35-38] Specifically, collagen-like peptides (CLPs) have been shown to mimic the tertiary structure of collagen, forming the characteristic triple-helix by using the proline-hydroxyproline-glycine (POG) repetitive units in the peptide sequence.[39-42] Modifying the design of such CLPs to both mimic collagen structure and incorporate moieties able to trap MG could result in a promising therapeutic approach that confers protection against MG damage. In this work, we developed and *in vitro* validated CLPs with MG trapping features (Fig. 1). The sequences were rationally designed in order to maximise the MG trapping capacity by adding arginine residues in specific positions, as this amino acid is one of MG's primary targets.[43, 44] Different permutations of arginine-containing peptides were designed and various characterizations performed, correlating triple-helix stability, arginine position and density, and MG consumption efficiency to define structure–property relationships and to identify the ideal peptide candidate for use as a MG-trapping therapeutic. Finally, the top peptide candidate was assessed using human cardiac endothelial cells in the presence of MG and was shown to protect the cells by reducing MG-H1 formation and oxidative stress.

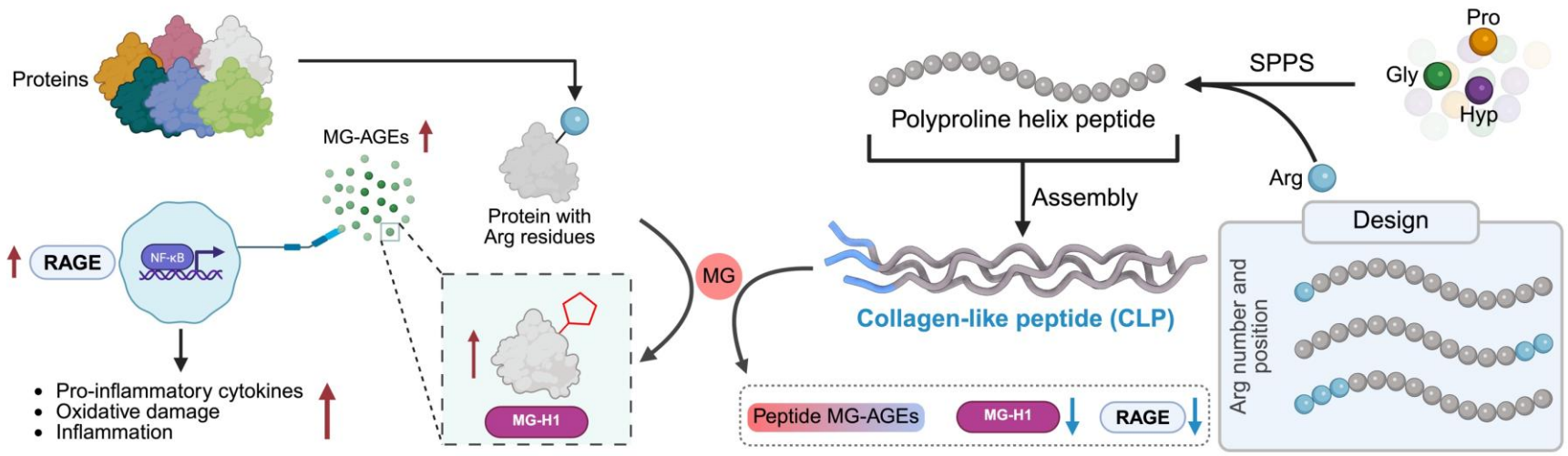



**Fig. 1**. **Schematic representation of the design for collagen-inspired peptides with arginine residues**. Under pathological conditions, increased levels of MG lead to protein glycation and the accumulation of MG-AGEs (primarily MG-H1) that promote RAGE expression, inflammation, and oxidative damage. In this work, we designed collagen-like peptides (CLP) using solid-phase peptide synthesis (SPPS) to trap MG, thus reducing protein glycation and protecting cells from its damaging effects.

## Results and Discussion

### Number and position of arginine modify triple helix formation and stability of CLPs

We recently reported that CLPs using $(POG)_n$ sequences with an *n* value between 6 and 10 result in a triple-helix formation that mimics the natural collagen structure and can be used for on-the-spot assembly of hydrogels for soft tissue and organ repair.[41] Thus, in the present study, we designed the core of our peptides using $(POG)_6$ to provide collagen-like assembly, as shown in Fig. 1. Sequences with the general structure **$NH_2$-XXX$(POG)_6$XXX-OH** were used, with X corresponding to the amino acid arginine (as MG-reactive moieties) or glycine (to maintain the helical folding). Table 1 contains the list of peptide sequences that were synthesized and some of the physical properties that were assessed. The peptide Pep1 corresponds to the – $(POG)_6$ – sequence with only glycine residues on both sides and constitutes the control peptide. Pep2 to Pep4 are the sequences with only 1 arginine residue at different positions, with Pep4 having an intentional disruption in the core POG sequence using the arginine. The peptides with 2 arginines in the structure are indicated as Pep5, Pep6, and Pep7. Finally, peptides with 3 arginines at different positions in the N- and C-termini are indicated as Pep8 to Pep11. The N-acetylated versions of specific peptides (Pep1, Pep2, Pep3, Pep8, and Pep11) were also included in the library to compare their glycation with the non-acetylated peptides. This was assessed since some MG-trapping capacity and reactivity were observed even for Pep1, which has no arginine residues (see Section 2.2 for more details). All peptides were synthesized by solid-phase peptide synthesis (SPPS) and purified to have a purity ≥ 98% (see Supplementary Table 1 for purity). Individual mass spectrometry ionization profiles for the different peptides are provided in the Supplementary information.

**Table 1**. Peptide sequence (with arginine residues indicated in red), molecular weight (MW), number of MG-trapping residues (arginine), melting temperature (Tm), and the fraction of peptide that is folded at 37 °C ($\alpha_{37\,°C}$) for the peptides that were synthesized.

| Code | Sequence | MW (g/mol) | #Arg | Tm ($R^2$) [a] | $\alpha_{37\,°C}$ (%) |
|---|---|---|---|---|---|
| Pep1 | $H_2N$-GGG**(POG)$_6$**GGG-OH | 1964.0 | 0 | 42 ± 2 (0.995) | 62 |
| Pep2 | $H_2N$-G**R**G**(POG)$_6$**GGG-OH | 2063.2 | 1 | 43 ± 1 (0.997) | 77 |
| Pep3 | $H_2N$-GGG**(POG)$_6$**G**R**G-OH | 2063.2 | 1 | 36 ± 1 (0.989) | 41 |
| Pep4 | $H_2N$- GGG**(POG)$_2$(PRG)(POG)$_3$**GGG-OH | 2007.1 | 1 | Two Tm [b] | 47 |
| Pep5 | $H_2N$-**RR**G**(POG)$_6$**GGG-OH | 2162.3 | 2 | 41 ± 1 (0.996) | 65 |
| Pep6 | $H_2N$-G**R**G**(POG)$_6$**G**R**G-OH | 2162.3 | 2 | 39 ± 3 (0.989) | 64 |
| Pep7 | $H_2N$-GGG**(POG)$_6$**G**RR**-OH | 2162.3 | 2 | 45 ± 1 (0.981) | 55 |
| Pep8 | $H_2N$-**RRR(POG)$_6$**GGG-OH | 2261.4 | 3 | 41 ± 1 (0.946) | 90 |
| Pep9 | $H_2N$-**RR**G**(POG)$_6$**G**R**G-OH | 2261.4 | 3 | 42 ± 5 (0.978) | 55 |
| Pep10 | $H_2N$-G**R**G**(POG)$_6$**G**RR**-OH | 2261.4 | 3 | 39 ± 2 (0.930) | 69 |
| Pep11 | $H_2N$-GGG**(POG)$_6$RRR**-OH | 2261.4 | 3 | 51 ± 2 (0.939) | 84 |
| AcPep1 | **Ac**-GGG**(POG)$_6$**GGG-OH | 2006.1 | 0 | 34 ± 1 (0.992) | 33 |
| AcPep2 | **Ac**-G**R**G**(POG)$_6$**GGG-OH | 2105.2 | 1 | 46 ± 1 (0.939) | 84 |
| AcPep3 | **Ac**-GGG**(POG)$_6$**G**R**G-OH | 2105.2 | 1 | 36 ± 2 (0.959) | 48 |
| AcPep8 | **Ac-RRR(POG)$_6$**GGG-OH | 2303.5 | 3 | 36 ± 3 (0.985) | 53 |
| AcPep11 | **Ac**-GGG**(POG)$_6$RRR**-OH | 2303.5 | 3 | 42 ± 1 (0.955) | 72 |

[a] Results were obtained by a sigmoidal model fitting. [b] Pep4 was observed to have two melting processes, with one occurring at a lower temperature of 25 ± 3 °C, and a second one at 62 ± 3 °C.

Circular dichroism (CD) spectroscopy confirmed the triple helix-like structure for all peptides, yielding the characteristic positive maximum at 220 nm and a minimum at 200 nm (see Supplementary Fig. 1). Fourier-transform infrared (FT-IR) spectroscopy corroborated the formation of triple-helix peptides by following the Gaussian fit of the amide I signal at ≈1630 $cm^{-1}$ (Supplementary Fig. 2). Thermal denaturation was monitored by following the CD signal at 225 nm while increasing the temperature; the resulting melting temperatures ($T_m$) are listed in Table 1 (with full traces provided in Supplementary Fig. 1). Most of the peptides exhibited a $T_m$ > 37 °C. Notably, the percentage of peptides that form a triple-helix structure at physiological conditions ($\alpha_{37\,°C}$), together with the associated $T_m$, indicates that the presence of arginine residues modifies the peptides' stability. As an example, Fig. 2A illustrates the influence of the C-terminal arginine. Specifically, Pep3, which carries a single C-terminal arginine, lacked a native (pre-transition) baseline and began to unfold even at 20 °C, indicating low stability ($T_m$ = 36 °C). Pep7 (with 2 C-terminal arginines) had improved stability with a flat baseline up to ~32 °C ($T_m$ = 45 °C). Finally, Pep11 (with 3 C-terminal arginine) remained almost fully folded until ~37 °C with a $T_m$ of 51±2 °C. Consequently, the fraction folded at 37 °C ($\alpha_{37\,°C}$) increased from 41% to 55% and to 84% when the peptide contained 1, 2, and 3 arginine on the C-terminal, respectively, highlighting the stabilizing effect of additional arginine in the sequence.

Molecular dynamics simulations support these experimental observations. In simulations initiated from the *stable conformation*, where a pre-organized hydrogen bond network is present, all peptides successfully maintain a well-formed triple-helical structure throughout the trajectory (Supplementary Fig. 3A-D). This finding suggests that the triple-helix configuration is a structurally accessible state for all peptides in the library when initiated from favorable initial conditions. However, when simulations are initiated from the *intermediate conformation*, clear differences emerge among the peptides (Supplementary Fig. 3E-H). Triple-helix formation is markedly enhanced for Pep3, Pep7, and Pep11, which carry C-terminal arginine residues. In contrast, Pep8, with arginine at the N-terminus, does not exhibit the same tendency to form stable triple helices. This behavior is further supported by measurements of the triple-helix radius, which show more compact and persistent structures for the C-terminal arginine peptides (Fig. 2B). Furthermore, the necessity and extent of structural maintenance vary among the peptides. Systems containing C-terminal arginine residues (Pep3, Pep7, and Pep11) exhibit elevated and persistent interchain hydrogen-bond populations across both simulations. This finding indicates enhanced

structural stability. Of particular significance are the subtle yet persistent variations observed within this group. Pep3 shows slightly fewer interchain hydrogen-bond counts and a less pronounced temporal persistence than Pep7 and Pep11, as evidenced by simulations. This gradation closely mirrors the experimentally determined melting temperatures reported in Table 1, further supporting the link between hydrogen-bond stability and thermal behavior. The comparison between Pep11, which contains three arginines at the C-terminus, and Pep8, which contains three arginines at the N-terminus, highlights arginine positioning, rather than mere abundance, as a key determinant of interchain organization, with direct implications for triple-helix formation and thermal stability. Solvent-accessible surface area (SASA) analyses further support these observations (Fig. 2C). Specifically, Pep3, Pep7, and Pep11 display a marked decrease in SASA values during the initial 20 ns of simulation, after which they remain stable, consistent with the maintenance of a compact and well-formed triple-helical structure. In contrast, Pep8 exhibits overall higher and more fluctuating SASA values throughout the trajectory, indicative of a less compact conformation and reduced structural persistence. This behavior further reinforces the notion that Pep3, Pep7, and Pep11 have a stronger intrinsic propensity to form and stabilize triple helices compared to Pep8. For the stable conformation, however, all peptides exhibit comparable SASA trends (characterized by low and steady values throughout the trajectory), although Pep8 maintains slightly higher absolute values. This indicates that, when initiated from a favorable orientation, all sequences can achieve and preserve a stable triple-helical structure, highlighting that the correct alignment of chains is sufficient to promote helix formation. Molecular dynamics simulations reveal, in fact, that Pep11 has a higher and more persistent number of hydrogen bonds throughout the trajectory compared to Pep8 (Fig. 2D and Supplementary Fig. 3), indicating a higher degree of conformational stability. The enhanced structural stability of these peptides may be attributed to favorable electrostatic interactions between the positively charged arginine side chains and the negatively charged carboxyl terminal, which promotes tighter packing and increased hydrogen bonding within the helix. These findings suggest that the number and positioning of arginine residues, particularly at the C-terminal end, play a crucial role in promoting interchain stabilization.

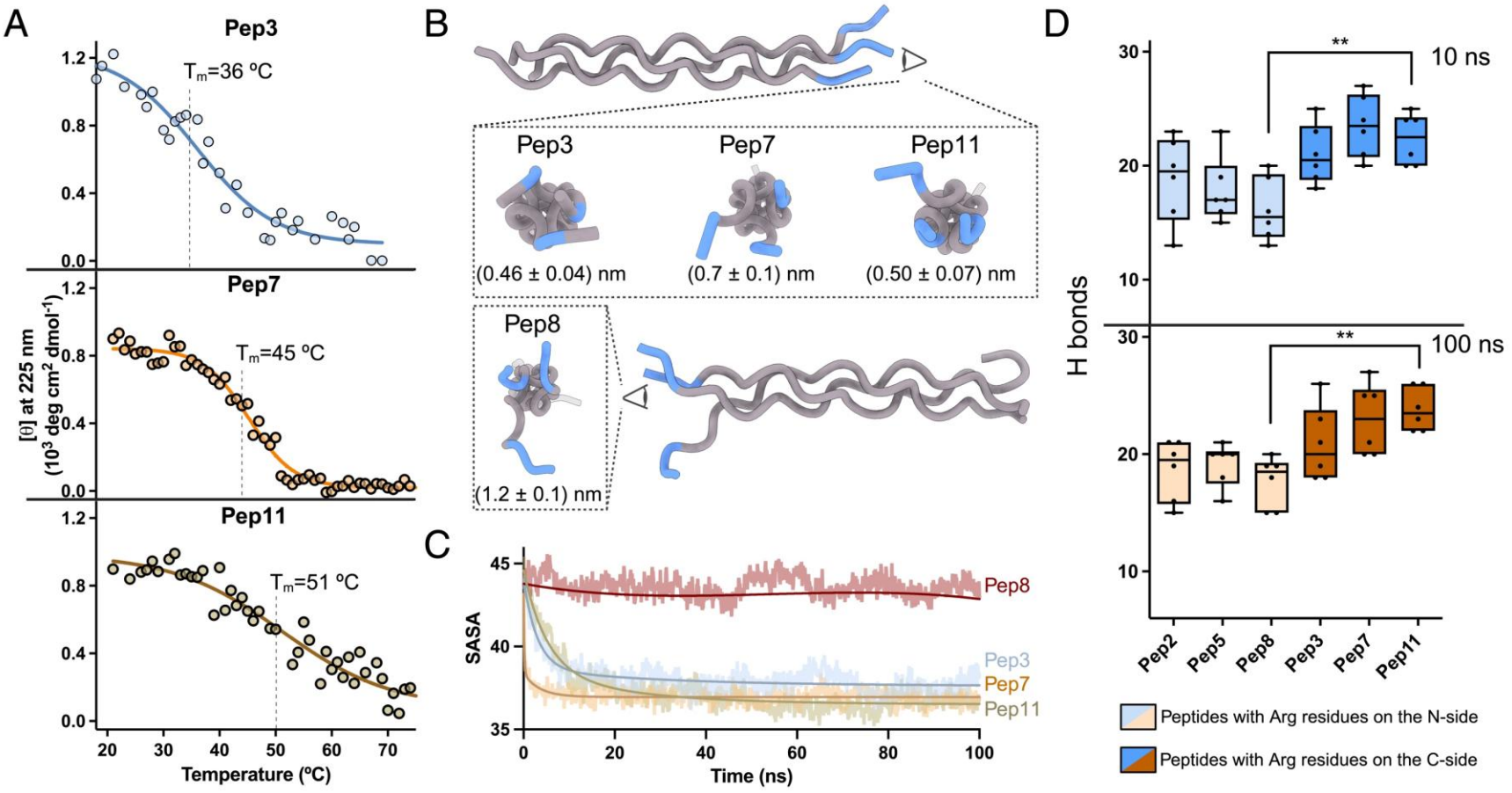



**Fig. 2**. **The number and location of arginine residues affect the stability of biomimetic self-assembling peptides**. A) Melting curves obtained for Pep3, Pep7, and Pep11; data points correspond to the experimental results, and the line represents the sigmoidal fitting. B) The last frame of the molecular dynamic simulations showing the top view of the structure of Pep3, Pep7, Pep8, and Pep11, and the corresponding average triple-helix radius calculated over the final 20 ns of the simulations for the arginine radius. C) SASA results for

pep3, pep7, pep8, and pep11. D) The number of interchain hydrogen bonds at 10 and 100 ns for Pep2, Pep3, Pep5, Pep7, Pep8, and Pep11; data represents the mean ± SD ($n = 6$; $^{**}p < 0.01$: $^{***}p < 0.001$; ANOVA followed by Tukey's test).

**MG-trapping efficiency of CLPs improved by increasing arginine residue numbers**

Having confirmed the helical structure and stability of the peptides, we next assessed their ability to trap MG. To determine the MG-trapping efficiency, as well as their reactivity, peptide solutions were incubated with an excess of MG and analyzed at different timepoints using two different methodologies (Fig. 3A). The *N*-acetyl-L-cysteine assay was used to evaluate the effect of the reactive groups in the peptides against MG (*i.e.*, trapping ability),[45, 46] and peptide consumption were quantified via high-performance liquid chromatography-mass spectrometry (HPLC-MS) to assess reactivity. The results of the *N*-acetyl-L-cysteine spectrophotometric method were further corroborated by HPLC-MS analysis (Supplementary Fig. 4).

MG consumption by the peptides in solution was quantified after 3 h and 48 h of incubation and expressed as molar equivalents of MG trapped per peptide equivalent (Fig. 3B). As expected, the consumption of MG increased with an increasing number of arginines per peptide. Interestingly, in addition to the number of arginines, their position within the peptide also played a key role in MG trapping at 3 h. Peptides with greater numbers of arginine at the C-terminal (rather than N-terminal), specifically Pep10 (3 arginine, 2 at C-terminal) and Pep11 (3 arginine at C-terminal), had the highest MG trapping capacity. MG consumption for the Pep10 and Pep11 peptides was comparable or better to that observed for the arginine-tripeptide control, used as a minimum peptide structure with the same number of reactive sites. This indicates that assembly of the triple-helix structure did not disrupt the MG trapping ability. Notably, the 48 h data suggest that all peptides reached a plateau for their MG trapping capacity and each arginine residue was shown to be able trap up to 2 equivalents of MG, which aligns with literature reports.[33, 43]

While the inclusion of arginine in the peptide structure was expected and shown to confer the ability to react with MG, it was also observed that the peptide control with no arginine (Pep1) also exhibited a small MG-trapping capacity of around 1.4 equivalents at 3 h, comparable to that of the free arginine amino acid. Although Pep1 lacks arginine residues, it contains an amine terminal that may be an MG-trapping site, since the reactive species (arginine) and the N-terminal amine are the only available targets in the peptides we tested, analogous to assays in the literature using di- and tripeptides.[47]

To better understand the trapping potential of the N-terminal amine, Pep1 was compared to its acetylated version (AcPep1), in which the N-terminal amine is modified by acetylation. The

quantification of Pep1 and AcPep1 in the presence of an excess of MG was performed by HPLC-MS to detect the amount of unreacted peptide that remained (Fig. 3C). The results indicated that AcPep1 remains almost constant (*i.e.*, no reactivity with MG), while Pep1 was ≈90% consumed (reacted with MG) at 3 h (Fig. 3D). After 24 h, no reactivity was observed for AcPep1, while Pep1 was entirely consumed and could no longer be detected (Supplementary Fig. 5). This indicates that the free N-terminal α-amine is the only nucleophilic site to react with MG under these conditions, generating dimer-like products.[48, 49] The same phenomenon related to the MG consumption by the free N-terminal could explain the differences in reactivity shown in Fig. 3B between other peptides and their acetylated versions. Specifically, it was observed that the non-acetylated peptides trapped approximately 1 more equivalent of MG compared to the acetylated versions after 3 h. After 48 h, the non-acetylated peptides (Pep2, Pep3, Pep8, and Pep11) consumed significantly more MG than their acetylated counterparts, indicating that acetylation of the N-terminal affects the longer-term MG-trapping capacity of the peptides.

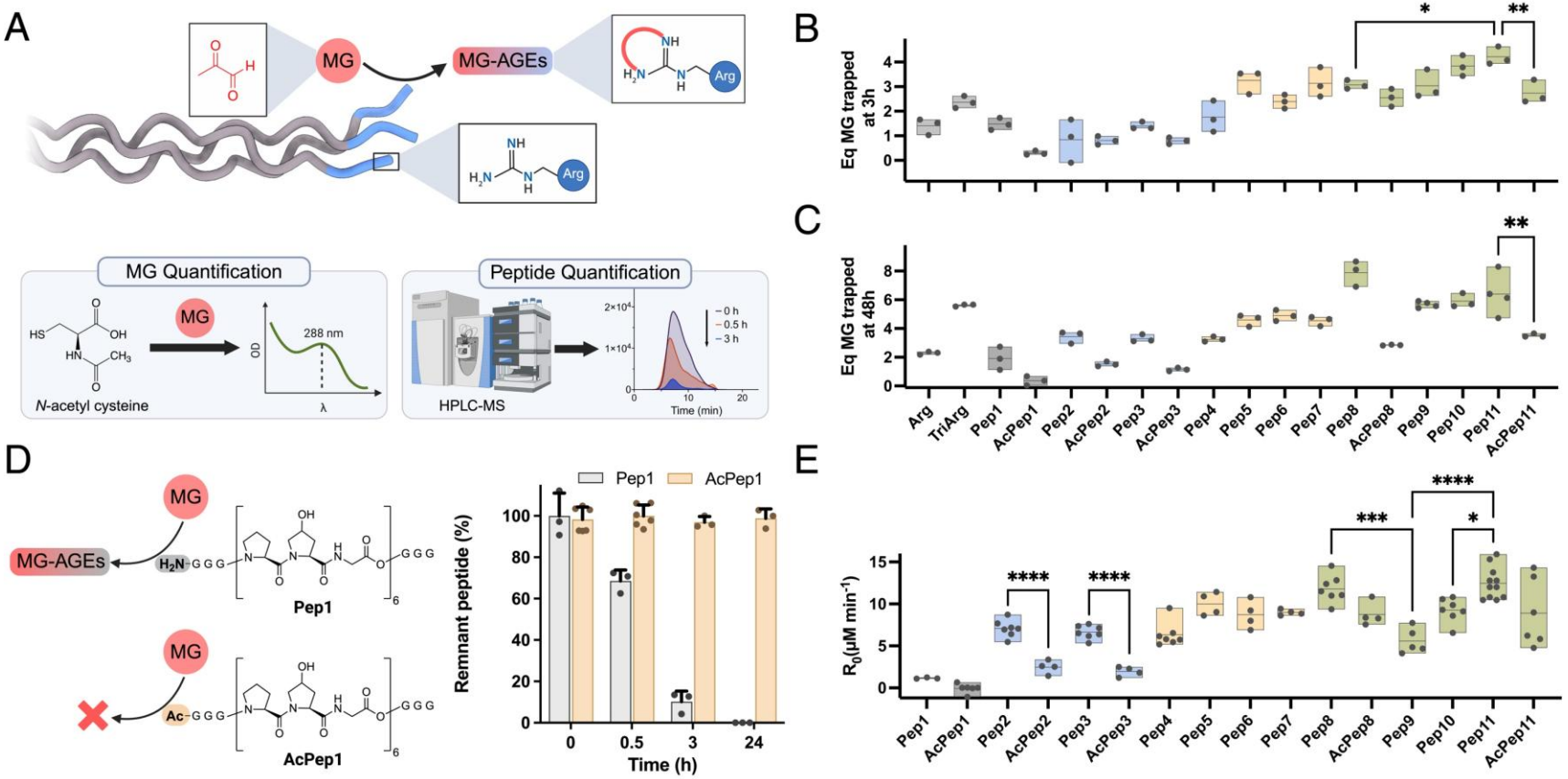



**Fig. 3. Analysis of the MG-trapping capacity of CLPs**. A) Schematic representation of the 2 methods used for analyzing the reaction of CLPs with MG to yield MG-AGEs (glycated product). The equivalents of MG trapped by the peptides after (B) 3h and (C) 48h, determined using the *N*-acetyl cysteine approach; data represents the mean ± SD ($n$ = 3-4; *$p < 0.05$; **$p < 0.01$; ANOVA followed by Tukey's test). D) Comparison of Pep1 and AcPep1 in terms of reactivity over time in the presence of an excess of MG, analyzed by HPLC-MS and presented as the percentage of peptide that remained unreacted. E) The consumption rate at 30 min ($R_0$, μM $min^{-1}$) for

peptides in the presence of excess MG calculated by following the main peak on HPLC-MS; data represents the mean ± SD ($n$ = 4-11; *$p$ < 0.05; **$p$ < 0.01; ****$p$ < 0.0001; ANOVA followed by Tukey's test).

**Conformational stability of CLPs contributes to their MG reactivity**

The influence of arginine number and position on the peptide's reactivity against MG was evaluated by monitoring the peptide consumption via HPLC-MS for a period of 30 min. From the kinetic traces (Supplementary Fig. 6), each peptide's initial consumption rate ($R_0$) was determined and expressed as the molar concentration of peptide consumed per minute (Fig. 3E). The $R_0$ value is higher for the peptides with more arginine residues, indicating that more reactive sites increase the consumption rate. Comparing the peptides with only 1 arginine residue (*i.e.*, Pep2 and Pep3), there was no observed difference in $R_0$, indicating that arginine position (C- vs. N-terminal) does not influence the early reaction phase for these peptides. Notably, acetylation of the N-terminal in these peptides (*i.e.*, AcPep2 and AcPep3) resulted in a >2-fold reduction in reactivity. This difference matches similar second-order rate constants reported for MG with primary amines ($k \approx 6.8 \times 10^{-2}$ $M^{-1}$ $s^{-1}$) and guanidinium groups ($k \approx 8.5 \times 10^{-2}$ $M^{-1}$ $s^{-1}$),[50] suggesting comparable initial reactivity of the free amine and arginine side chain. The molecular analysis of AcPep2 products also corroborated both first- and second-stage adduction events, yielding characteristic m/z signals for the expected AGEs that are formed (Supplementary Fig. 7).

For the peptides containing 3 arginines, their position modified the initial consumption rate, where those peptides with arginine distributed on both sides (Pep9 and Pep10) show a significantly lower $R_0$, compared to Pep8 (3 arginines on N-terminal) and Pep11 (3 arginines on C-terminal). However, no differences were observed between Pep8 and Pep11, having similar $R_0$ of 11.8 ± 1.6 and 12.5 ± 1.9 μM $min^{-1}$, respectively. For these peptides, acetylation did not modify the consumption rate as no differences in initial reactivity were observed between Pep8 and AcPep8 and between Pep11 and AcPep11. These results suggest that the initial rate ($R_0$) does not depend on the position of the arginine residues in acetylated peptides during the first MG-trapping step. This implies that the residues behave equivalently, without apparent influence from their number, position, or peptide folding. This behavior is consistent when comparing either AcPep2 and AcPep3 (one arginine) or AcPep8 and AcPep11 (three arginines), since in both cases the position of the Arg residues (N- or C-terminal) did not affect the $R_0$.

Further molecular dynamics simulations were performed and analyzed for the peptides containing 3 arginine residues (Pep8, Pep9, Pep10, and Pep11). Results for Pep11 provide a good demonstration of how maintaining a stable triple-helical conformation directly contributes to the spatial organization of the functional residues. Structural analyses revealed that the preserved

architecture of Pep11 facilitates the formation of a cluster of arginine residues (Fig. 4A), consistently positioned near the C-terminal region. This phenomenon arises from the constrained geometry of the helix, leading to a localized accumulation of positive charge. Such arginine-rich microenvironments have been previously described in the literature as key determinants in enhancing peptide reactivity, especially towards electrophilic targets. For example, the concentration of guanidinium groups within a limited solvent-accessible volume facilitates chemical trapping processes.[51, 52] In the case of Pep11, the stable folding pattern ensures that the three arginine residues are not only correctly oriented but also brought into close spatial proximity, effectively forming a functional arginine cluster. This localized arrangement is hypothesized to generate a positively charged hotspot, contributing to the enhanced MG reactivity observed for Pep11. The capacity to sustain this clustering over an extended period is a direct outcome of the maintained triple-helical structure, which furnishes a stable scaffold for positioning reactive side chains. In contrast, although Pep8 also contains 3 arginine residues, their position on the N-terminal of the peptide leads to a less stable conformation during the simulations. The hydrogen bonding network is reduced, and no persistent spatial clustering of the arginine side chains is observed, as confirmed by the fraction of assembly data (Fig. 4B). This may explain why, although Pep8 and Pep11 have similar initial reactivity with MG, Pep11 is superior in its overall MG-trapping capacity. The behaviors of Pep9 and Pep10 (3 arginine residues distributed on both N- and C-termini) are noteworthy, as they exhibit significant structural destabilization throughout the simulations. The two peptides progressively lose their triple-helical organization, ultimately adopting largely disordered conformations.

Pearson's correlation matrices were prepared to summarize and link the different experimental results and the synthesized peptides' structural features (Fig. 4C; only those correlations with a value > 0.7 are highlighted). For the non-acetylated peptides, there was a high correlation between the number of arginine residues in the peptide structure and the consumption of MG at 3 and 48h (0.92 and 0.94, respectively). In addition, the MG consumption at 3h showed a strong correlation with peptides containing arginine moieties on the C-terminal (0.71), and a weak correlation with those on the N-terminal (0.25). However, this relationship changes over time with a decrease at 48h in the correlation between MG consumption and peptides with arginine residues on the C-terminal (0.40), and an increase for those on the N-terminal (0.62), compared to the 3h values. Interestingly, these correlations differ when assessing the results for the acetylated

peptides. With acetylation, the consumption of MG at 3h exhibited a moderate correlation with the position of arginine on the C-terminal (0.56) or on the N-terminal (0.46). At 48h, the consumption of MG showed a slight increase, but still a moderate correlation with the position of arginine on the C-terminal (0.62), and a weaker correlation with those on the N-terminal (0.38). These correlation results demonstrate that the number and position of arginine residues in collagen-like peptides are key points in designing effective MG-trapping structures. Taken together, these studies identify that conformational stability is an important factor in determining the peptide's reactivity with MG.

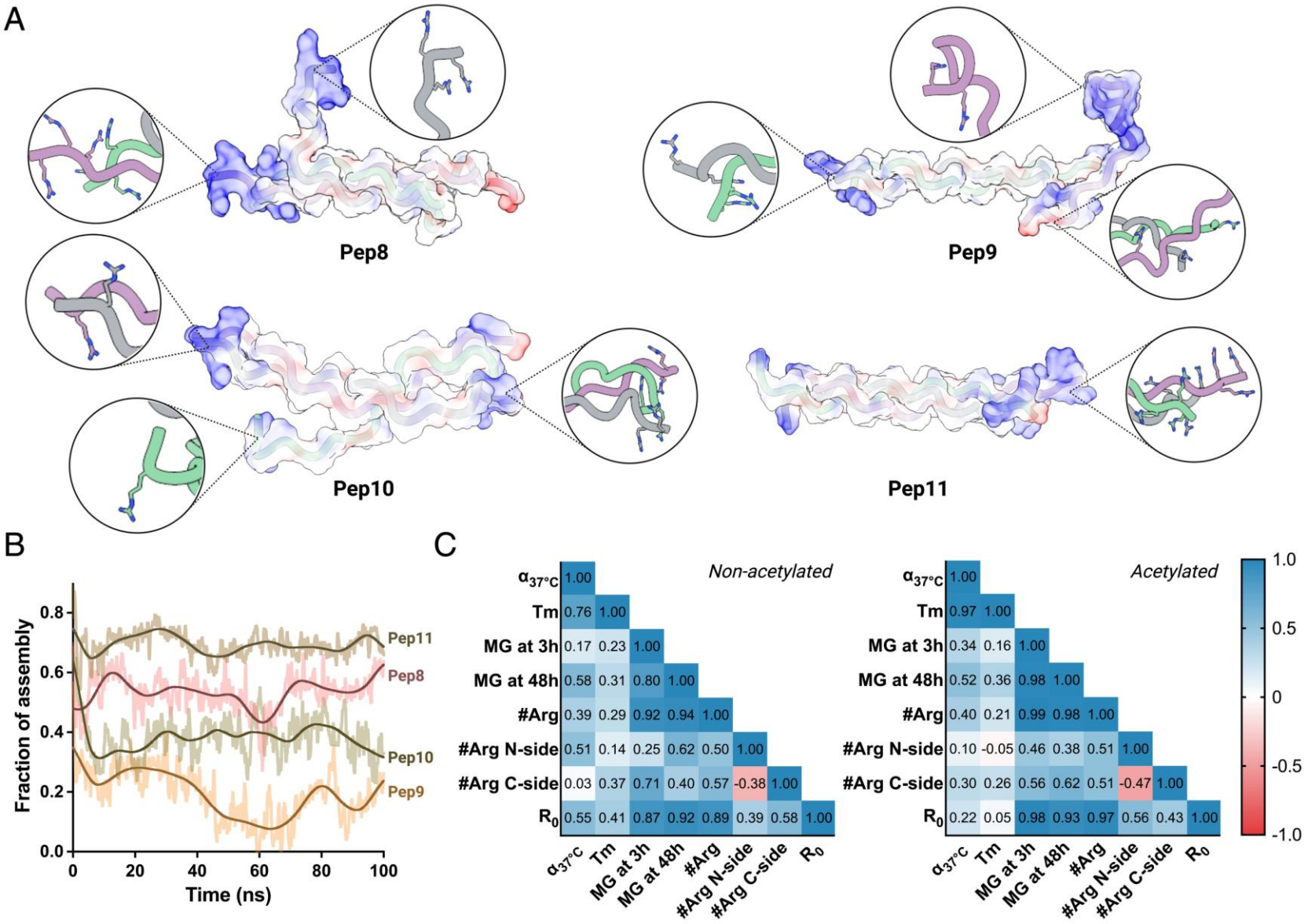

A
Pep8
Pep9
Pep10
Pep11
B
Fraction of assembly
Time (ns)
Pep11
Pep8
Pep10
Pep9
C
Non-acetylated
Acetylated
α37°C
Tm
MG at 3h
MG at 48h
#Arg
#Arg N-side
#Arg C-side
R0
1.0
0.5
0
-0.5
-1.0

**Fig. 4. Influence of the electrostatic surface of CLPs on structural and functional features**. A) Electrostatic surface representation of the last frame of molecular dynamics simulations performed for CLPs containing 3 arginine (Pep8, Pep9, Pep10, and Pep11), with positively charged regions shown in blue and negatively charged areas shown in red. The side chains of arginine residues are highlighted in the magnified areas. B) Molecular dynamics simulation results for the average peptide fraction with triple helix assembly over time for peptides Pep8, Pep9, Pep10, and Pep11. C) Pearson's correlation matrices from the experimental results and structural features for non-acetylated and acetylated peptides.

**Pep11 protects endothelial cells from MG damage *in vitro***

Considering all the structure/function properties for the CLPs presented above, Pep8 and Pep11 (3 arginine residues) demonstrated the best MG-trapping capacity over time. As such, these 2 peptides were selected for *in vitro* biocompatibility testing. Notably, Pep11 (250 μM) did not exhibit cytotoxicity to human cardiac microvascular endothelial cells (HCMECs), whereas Pep8 showed increasing toxicity between 50 and 250 μM (Supplementary Fig. 8). Interestingly, there was no toxic effect when cells were treated with AcPep8 (Supplementary Fig. 8), suggesting that the sequence arrangement, conformational differences, or N-acetylation can affect the peptide's cytotoxic property. While acetylation of Pep8 reversed its cytotoxic effect, it also reduced its MG-trapping capacity (Fig. 3C). Therefore, Pep11 was selected for further *in vitro* testing because it showed no toxicity and exhibited the highest stability, MG reactivity, and MG-trapping capacity.

To this end, HCMECs were exposed to MG ± Pep11 treatment, and a Live/Dead assay was performed to assess cell viability. The results showed an increase in cell death in the presence of MG, which was rescued by treatment with Pep11, with viability restored to levels equivalent to the control group that did not receive MG or peptide (Fig. 5A, B). This indicates that the MG-trapping ability of Pep11 was able to protect HCMECs from MG-induced cell death. MG exposure is known to trigger an increase in the expression of the receptor for advanced glycation end-products (RAGE) on the cell surface.[53, 54] Therefore, immunohistochemistry for RAGE was performed to further investigate the MG-trapping capacity of Pep11 (Fig. 5C). Staining results revealed that the mean intensity of RAGE in the Pep11 group was significantly lower than in the MG alone group (Fig. 5D). Moreover, no difference in RAGE expression was found between the Pep11 group and cells seeded in normal culture medium without MG (Fig. 5E), suggesting that Pep11 was able to trap MG, preventing its interaction with cells and subsequent RAGE signaling. Lastly, we assessed the cellular expression of MG-H1 and Glo1 in the HCMECs by western blot. Pep11 treatment was observed to significantly reduce MG-H1 levels in the cells compared to those treated with MG alone (Fig. 5F), and there was a trend for increased Glo1 expression in the Pep11-treated group compared to the other groups (Fig. 5G). Overall, these results demonstrate the ability of Pep11 treatment to trap MG and protect cells from its negative effects by preventing MG-H1 accumulation and RAGE expression and maintaining cell viability.

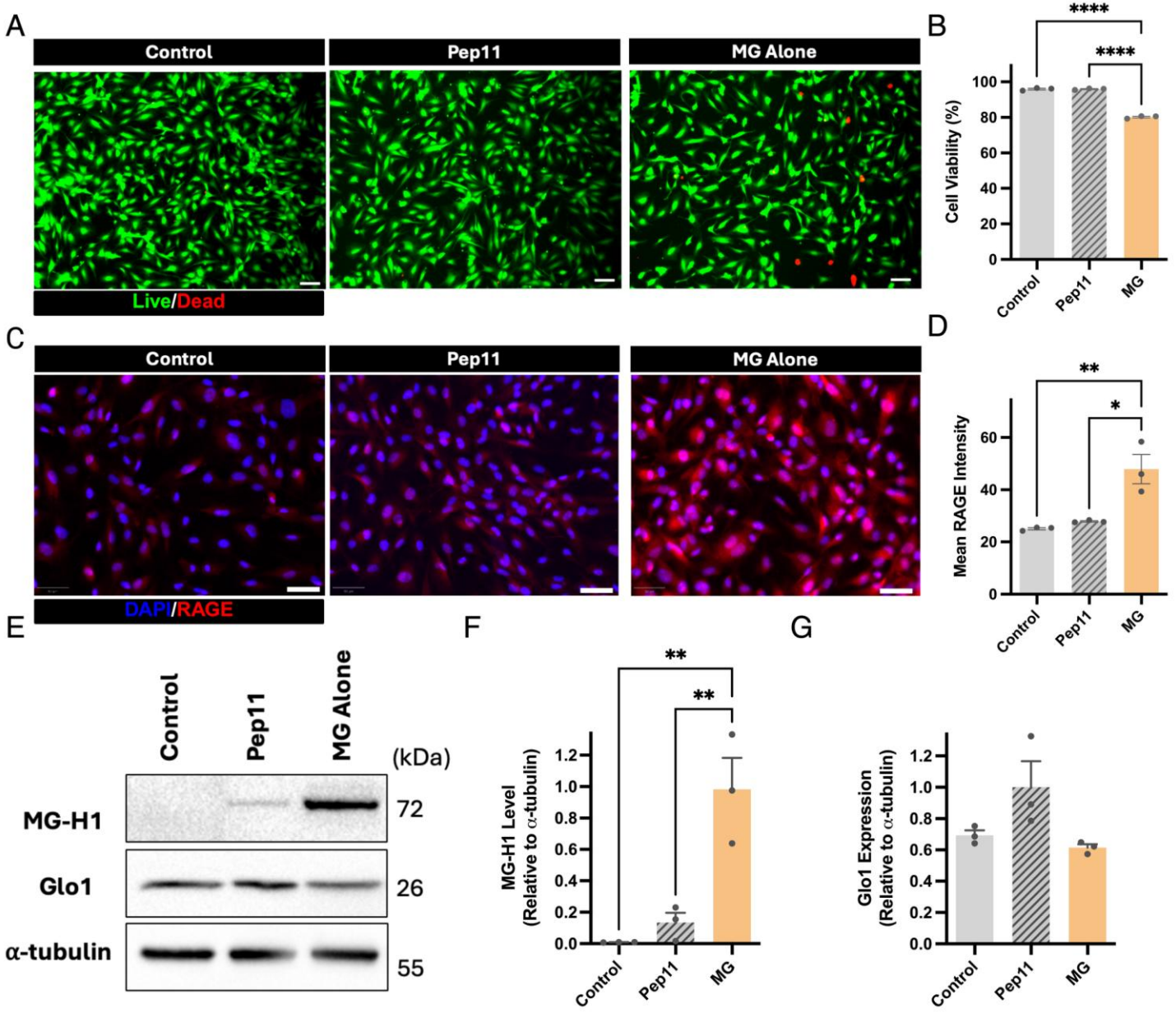

A
Control
Pep11
MG Alone
Live/Dead
B
****
****
Cell Viability (%)
100
80
60
40
20
0
Control
Pep11
MG
C
Control
Pep11
MG Alone
DAPI/RAGE
D
**
*
Mean RAGE Intensity
60
40
20
0
Control
Pep11
MG
E
Control
Pep11
MG Alone
(kDa)
MG-H1
72
Glo1
26
α-tubulin
55
F
**
**
MG-H1 Level
(Relative to α-tubulin)
1.2
1.0
0.8
0.6
0.4
0.2
0.0
Control
Pep11
MG
G
Glo1 Expression
(Relative to α-tubulin)
1.2
1.0
0.8
0.6
0.4
0.2
0.0
Control
Pep11
MG

**Fig. 5**. **Pep11 treatment protects cells from MG damage *in vitro***. A) Representative Live/Dead assay images of HCMECs after 24 h of culture with different treatments (scale bar =100 μm). B) Quantification of HCMEC viability ($n = 3$ per group). C) Representative immunofluorescence images of RAGE staining of HCMECs after 24 h of culture with different treatments (scale bar = 50 μm). D) Quantification of the mean fluorescence intensity of RAGE. E) Representative western blot images for MG-H1 and Glo1 expression in HCMECs after 24 h of culture with different treatments. Quantification of the western blot results for (F) MG-H1 and (G) Glo1 ($n = 3$ per group). Data are presented as the mean ± SEM. *$p < 0.05$; **$p < 0.01$; ****$p < 0.0001$. Differences between groups were determined by a one-way ANOVA with Bonferroni correction.

To further confirm that the MG-trapping properties of Pep11 are responsible for its protective effects on endothelial cells, it was compared to the AcPep1 control peptide. The AcPep1 peptide has no capacity to trap MG as it contains no arginine, and the reactivity of the N-terminal has been nullified by the acetylation. For consistency, the acetylated version of Pep11 was used in these experiments to eliminate the acetylation status as a possible factor in any observed differences. HCMECs were cultured with no peptide, AcPep11, or AcPep1 in the presence of MG in culture media. The results of a Live/Dead assay showed a loss in viability when cells were treated with MG, which was rescued by treatment with AcPep11, but not by AcPep1 (Supplementary Fig. 9A, B). This indicates that the MG-trapping ability of AcPep11 was able to protect HCMECs from MG-induced cell death. Furthermore, as was seen for Pep11, the mean intensity of RAGE in cells treated with MG + AcPep11 was significantly lower than those exposed to MG alone, while the AcPep1 treatment failed to reduce RAGE expression (Supplementary Fig. 9C, D). Moreover, no difference in RAGE expression was found between the AcPep11 group and control group, suggesting that AcPep11, but not AcPep1, was able to trap MG and prevent it from activating RAGE signaling.

Lastly, we assessed the cellular expression of MG-H1 and Glo-1 in the HCMECs by western blot. The results revealed that AcPep11 treatment significantly reduced MG-H1 levels in MG-exposed cells compared to those treated with MG alone or MG + AcPep1 (Supplementary Fig. 9F). Moreover, Glo1 expression in the AcPep11-treated group was increased compared to the other experimental groups (Supplementary Fig. 9G). Altogether, given that AcPep1 was ineffective, these findings indicate that the capacity for (Ac)Pep11 to trap MG is key in its ability to protect cells from MG-induced damage in cultured endothelial cells.

**MG-modified Pep11 does not increase RAGE expression**

AGEs themselves can promote RAGE expression and subsequently activate RAGE signalling.[55, 56] The results presented in Fig. 5C and D showed no increase in RAGE expression in cells that were treated with MG + Pep11, suggesting that the resultant MG-modified Pep11 does not act like an AGE. To confirm this, we directly examined the effect of glycation products from Pep11 (Pep11-AGEs) on RAGE expression in endothelial cells compared to conventional AGEs from human serum albumin protein (HSA-AGEs). Glycation product formation was induced by incubating Pep11 and HSA with MG (Fig. 6A). HPLC-MS analysis confirmed ~40% conversion

from Pep11 to Pep11-AGEs (Fig. 6B), finding MG-H1 and also other intermediates of an MG/arginine reaction, such as dihydroxyimidazolidine (MG-DH), carboxyethylarginine (CEA), argpyrimidine (APY), and MG-derived imidazolium crosslink (MODIC) (Fig. 6C).[57, 58] For more details about the extracted ions for each glycation product, see Supplementary Fig. 10. Meanwhile, HSA glycation was confirmed by dot blot (Supplementary Fig. 11A).

In culture, the addition of HSA-AGEs to the media reduced the viability of endothelial cells, whereas Pep11-AGEs did not induce death (Fig. 6D and Supplementary Fig. 11B). Similarly, the presence of HSA-AGEs promoted RAGE expression in the endothelial cells, while Pep11-AGEs did not have this effect (Fig. 6E, F). These findings indicate that the glycation products formed by the reaction of MG with Pep11 are not biologically equivalent to those formed with HSA and have a limited ability to promote RAGE expression in endothelial cells. This suggests that arginine glycation in our stable peptide framework is not sufficient to generate a ligand capable of promoting a detectable RAGE-associated response. This fits with the recently reviewed concept that the biological effects of glycation products depend not only on the presence of glycation itself, but also on the nature of the modified substrate.[49] Since the structural features of AGEs that control its interactions with RAGE remain incompletely defined, Pep11 may provide a useful framework for exploring anti-glycation strategies and, potentially, for limiting MG-driven cellular dysfunction.

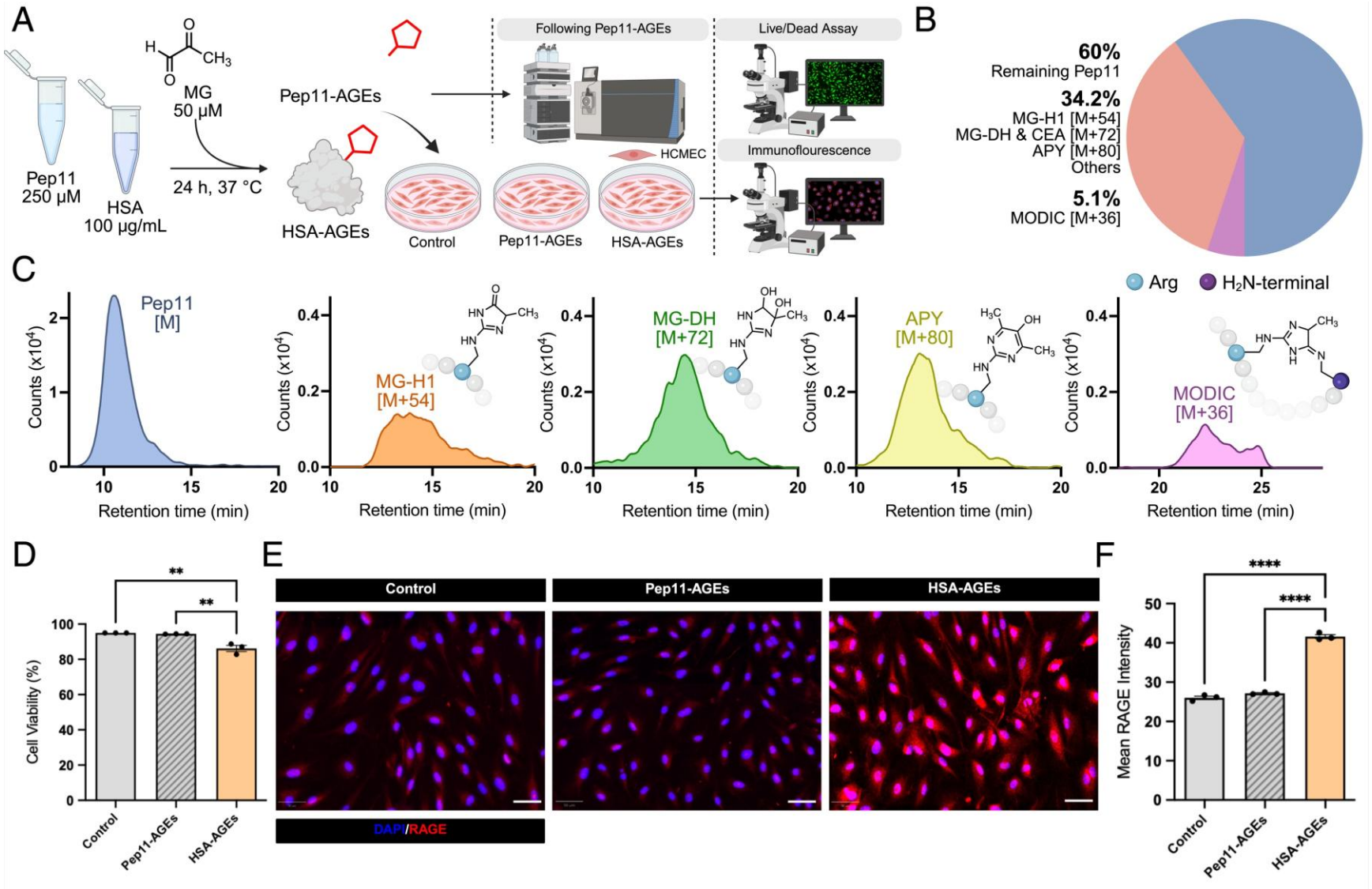



**Fig. 6**. **Pep11-AGEs do not increase RAGE expression *in vitro***. A) Schematic representation of the glycation process for Pep11 and HSA. B) Conversion (%) of Pep11 to Pep11-AGEs obtained from the peak area in the chromatogram of the incubated sample. C)

Representative extracted ion chromatograms of the different Pep11-AGEs observed. D) Quantification of HCMEC viability ($n = 3$ per group). E) Representative immunofluorescence images of RAGE staining of HCMECs after 24 h of culture with different treatments (scale bar = 50 μm). F) Quantification of the mean fluorescence intensity of RAGE. Data are presented as the mean ± SEM. $^{**}p < 0.01$; $^{****}p < 0.0001$. Differences between groups were determined by a one-way ANOVA with Bonferroni correction.

## Conclusions

The accumulation of long-lasting MG-AGEs that are produced spontaneously in the body are important contributors to the aging process and in the pathology of diseases that affect the brain, heart, liver, kidneys, pancreas, and immune system. In addition to its detrimental cellular effects, MG targets the long-lived proteins of the extracellular matrix, with a high affinity for collagen, and specifically its arginine residues. This provided the inspiration for designing the collagen-based MG-trapping peptides reported herein for use as therapeutics for reducing MG-induced damage in aging and disease.

Structural characterization of the different CLPs demonstrated that the stability of the triple helix formed depends on the number and location of the MG-reactive arginine residues in the peptide chain. By locating arginine(s) close to both terminals, stable and well-folded collagen-like peptides with up to 3 arginine residues were obtained. The greatest stability was achieved by the incorporation of 3 arginine residues on the C-terminal (*i.e.*, Pep11), which could be attributed to increased interchain hydrogen bonding. Notably, the MG-trapping capacity of the peptides was also dependent on the number and location of the arginines. Pep11, with its 3 arginine residues on the C-terminal exhibited the greatest ability to react with and trap MG over a period of 48 h. This feature is likely related to the superior stability of Pep11 and its conformation that produces a positively charged localized arginine cluster for enhanced MG reactivity.

The *in vitro* results confirmed that Pep11 was able to protect cells from the negative effects of MG. Specifically, treatment with Pep11 resulted in less intracellular MG-H1 accumulation, a reduction in RAGE expression and superior viability for endothelial cells cultured in the presence of MG. These findings warrant future investigation of Pep11's MG-trapping protective effects in relevant animal models of aging or disease. Given the versatility of peptides, one can envision many different strategies for the administration of Pep11 therapy depending on the condition being treated. For example, Pep11 could be administered alone, or incorporated within a hydrogel or nanoparticle, for delivery directly into the target tissue or through the circulation.

Collectively, these results demonstrate the successful design of a collagen-like peptide containing arginine that was stable, that possessed excellent MG-trapping capacity and that could protect cultured cells from MG damage. This makes it a promising therapeutic approach for trapping MG and limiting its negative effects on aging and disease.

## Methods

### Peptide synthesis

The peptides were synthesized using microwave-assisted Fmoc solid-phase peptide synthesis (SPPS)[59] in a Liberty Blue automated system, using Fmoc-protected amino acids and low-loading Wang resin, all purchased from CEM. Briefly, the required amount of resin was swelled in dimethylformamide for 5 min. Next, Fmoc deprotection was performed with 20% piperidine at 60 °C for 180 s. To add the proline, hydroxyproline, and glycine to the peptide sequence, standard *N,N'*-Diisopropylcarbodiimide (DIC)/Oxyma Pure coupling cycles were run at 60 ºC for 360 s. The arginine motifs were added using double coupling cycles, twice at 60 ºC for 360 s. Peptides were cleaved from the resin and deprotected with TFA/TIS/$H_2O$ (95/2.5/2.5% v/v) at 42 °C for 60 min and then precipitated in -20 °C diethyl ether. The crude peptide products were then dried under nitrogen overnight and purified by HPLC in an Agilent 1290 Infinity II Preparative LC/MSD System in preparative mode, with a 100x30 mm C18 column at 50 mL/min. Peptide purity and identity were confirmed using the same piece of equipment in analytic mode with a 100x4.6 mm C18 column at 0.8 mL/min. A purity of ≥98% was determined through HPLC peak analysis. Finally, peptides were freeze-dried and stored for further characterization. Table 1 and Supplementary Table 1 summarize the detailed mass spectrometry data and peptide purity for each peptide. Individual spectrum images are provided in the Supplementary information (pp S13-S28).

### Spectroscopic peptide characterization

Circular dichroism (CD) spectra were collected on a JASCO J-810 CD Spectrometer (JASCO, USA) with a bandwidth of 1.0 nm in the ultraviolet region (190–260 nm) using a 0.5 mm optical pathway quartz cuvette. The dichroic angle was measured with a resolution of $5x10^{-4}$ mdeg under an $N_2$ gas flow pressure of 40 psi. To reduce noise, 10 scans were averaged per sample. CD spectra were measured at 25 ºC using an MPTC-490S accessory to regulate the temperature. All peptide solutions were at a concentration of 200 µM in 1 mM phosphate buffer (pH 7.4) and were incubated at 4 ºC for 1 h to improve the folding. For the melting curves, the CD signal at 200 nm was recorded at temperatures ranging from 10 to 70 ºC. The temperature was increased at a rate of 2 ºC/min, with a delay time of 30 s for each measurement. Finally, a non-linear sigmoidal curve fit with a Boltzmann adjustment was used to fit the CD signal measurements, and the melting temperature

($T_m$) was determined from the inflection point of the melting curve using the general equation for a sigmoidal curve, as follows:

$$y = \frac{A_1 - A_2}{1 + e^{(x - x_0)/dx}} + A_2 \qquad \text{(eq 1)},$$

where $x_0$ corresponds to the curve's inflection point, taken as $T_m$.

The fraction of each peptide that was folded ($\alpha_{37\,^\circ C}$) was calculated from the melting curves as follows:

$$\alpha_{37\,^\circ C} = \frac{([\theta]_{37\,^\circ C} - [\theta]_U)}{([\theta]_F - \theta_U)} \qquad \text{(eq 2)},$$

where $[\theta]_{37\,^\circ C}$ is the molar ellipticity at 37 °C, $[\theta]_F$ is the molar ellipticity when the peptide is fully folded (starting melting curve condition), and $[\theta]_U$ is the molar ellipticity of the fully unfolded peptide (final melting curve condition).

The FTIR spectra were recorded using a Nicolet iS5 FT-IR with an attenuated total reflectance iD7 accessory and a diamond crystal. All spectra were measured at room temperature in the 4000-500 $cm^{-1}$ range. To reduce noise, 64 scans were averaged at a resolution of 4 $cm^{-1}$. Each freeze-dried peptide (less than 1 mg each) was applied to the spectrometer. The spectra of the amide I region (1750-1550 $cm^{-1}$) were then fitted by multiple Gaussian peaks.

**Glycation protocol for peptide consumption**

The glycation process was conducted by incubating the CLPs at a concentration of 250 µM in a 100 mM sodium phosphate buffer (pH 7.4) solution containing 5 mM MG at 37 °C. For the glycation kinetics of the peptides, 250 µL aliquots were collected at various time points (0, 5, 10, 15, 30, 60, 120, and 180 min). Residual MG was quenched by adding 250 µL of 40 mM aminoguanidine. The samples were stored at -80 °C for subsequent analysis.

**Analysis of MG-modified peptides**

The MG glycation products for the various peptides were determined by HPLC-mass spectrometry (HPLC-MS) analysis. Peptide samples (160 µL of each) were injected into an Agilent 1290 Infinity II LC/MSD system in analytical mode, and run using a 50 x 2.10 mm, 100 Å, C18 Kinetex column

(Phenomenex), with a flow rate of 0.9 mL/min at 45 °C. The mobile phases consisted of 5% acetonitrile (ACN) in water with 0.1% formic acid (FA) and 0.01% trifluoroacetic acid (TFA) for phase A, and 95% ACN in water acidified with 0.1% FA and 0.01% TFA for phase B. Chromatography was performed in gradient mode, starting with an isocratic step of 100% phase A for 4 min, followed by a gradient increase of phase B at a rate of 0.018%/min over 54 min to reach 1% phase B. The cleaning step involved increasing phase B to 80% from minutes 61 to 63, and the initial conditions were restored at minute 65. Under these conditions, the peptide and its glycation products were resolved.

In the MS detector, ionization was performed at 5000 V in positive ion mode, using single-ion monitoring with a scan range of 300 to 3000 m/z. Peptide consumption was determined using the ion filter function of Autoscale-MSD software (Agilent) by analyzing each peptide's second- and third-charged states. The glycation products were detected similarly with mass increases of +45 and +54 m/z.[43] The areas under the curves were used to quantify the peptide concentration over time.

**Methylglyoxal trapping assay**

MG trapping by CLPs was assessed at 0, 0.5, 3, 24, and 48 h using an *N*-acetyl-L-cysteine assay.[45] Samples were prepared with 250 µM peptide and 5 mM MG in 100 mM phosphate buffer (pH 7.4). A control using only 5 mM MG in 100 mM phosphate buffer (pH 7.4) was also prepared. At each time interval, samples for each peptide were removed and a 1:1 dilution was performed with either 100 mM phosphate buffer (pH 7.4), as a baseline, or 20 mM N-acetyl-L-cysteine and incubated for 5 min at room temperature. The optical density (OD) of each sample was then measured at 288 nm with a SpectraMax M2 microplate reader using a 5 mm quartz cuvette. The difference in OD between the N-acetyl-L-cysteine and phosphate buffer samples was used to calculate the remaining MG concentration. A linear calibration curve was constructed using OD at 500 µM, 1000 µM, 1500 µM, 2000 µM, 2500 µM, and 3000 µM MG to correlate OD and the remaining sample MG concentration ($R^2 = 0.998$).

**Molecular dynamics simulations**

The structural behaviour of the full peptide library was investigated through the execution of molecular dynamics (MD) simulations, which was enabled by support provided by the Digital Research Alliance of Canada (alliancecan.ca). Given the variability in helical propensity among

the different peptides, three independent simulation sets were performed for each system, starting from distinct initial conformations to ensure a broader sampling of the conformational landscape. The selected starting structures were devised to symbolize increasingly stable conformational states as follows: (i) an *unstable conformation*, where proline residues are oriented inward, thereby hindering the formation of stabilizing hydrogen bonds; (ii) an *intermediate conformation*, in which proline residues face outward, but no hydrogen bonding is yet established; and (iii) a *stable conformation*, characterized by an increased presence of hydrogen bonds, indicative of a pre-organized helical structure.

For each system, three 100-ns production simulations were executed in explicit solvent using the TIP3P water model. Simulations were performed with the CHARMM force field implemented in the GROMACS software suite. All simulations were executed under isothermal–isobaric conditions (constant number of particles, constant temperature, and constant pressure), with periodic boundary conditions applied in all directions. Prior to the production phase, each system underwent energy minimization followed by a 100 ps equilibration at 300 K, using a time step of 0.5 fs. Production runs were then conducted using a 2 fs time step. Long-range electrostatic interactions were treated using the particle mesh Ewald method,[60, 61] with a real-space cut-off of 1.2 nm. The same cut-off was applied to van der Waals interactions. Temperature was maintained using the velocity rescaling thermostat,[62] with a coupling constant of 0.6 ps. Pressure was controlled using the Berendsen barostat[63] with isotropic coupling and a time constant of 1 ps. Hydrogen bonding and SASA analyses were performed using standard GROMACS tools, while the fraction of assembly was evaluated through an in-house developed python script. The radius of the triple helices was quantified by tracking the spatial arrangement of the terminal arginine residues over the course of the MD simulations. For each frame, the global helical axis was determined, and the positions of the terminal markers were projected onto a cylindrical coordinate system centered on this axis. The radial displacement of the C-terminal (or N-terminal) arginine residues was used as a geometric descriptor of helix separation at the termini. The three peptide chains were identified based on their angular orientation around the helical axis, allowing measurement of the end-to-end expansion for each chain independently. Molecular visualizations and structural representations were generated using UCSF Chimera.

**Cell viability assay**

Human cardiac microvascular endothelial cells (PromoCell, cat#:C-12285) were cultured in tissue culture plates and maintained in Endothelial Cell Growth Medium MV2 (supplemented with Supplement Mix (PromoCell, cat#:C-22022) and 1% penicillin/streptomycin until they reached around 90% confluency. Cells were then seeded into 48-well plates with a seeding density of 2.5 $\times 10^4$ cells per well and treated with 0 μM, 50 μM, 100 μM or 250 μM of peptide (acPep1, Pep8, acPep8, Pep11 or acPep11) ± 50 μM of MG in MV2 medium. To test the cytotoxicity of Pep11-AGEs, cells were treated with 250 μM Pep11-AGEs or 100 μg/ml HSA-AGEs as a positive control. After 24 h, cell viability was assessed using a LIVE/DEAD™ Viability/Cytotoxicity kit (Calcein-AM and Ethidium Homodimer-1; ThermoFisher Scientific, Cat# L3224), according to the manufacturer's instructions. Fluorescence imaging was performed using a Zeiss microscope, and the number of live and dead cells was quantified using ImageJ2 software (NIH, USA). Each experiment was repeated three times, and images of three random fields-of-view were taken for each experimental group.

**Immunofluorescence staining**

HCMECs were seeded into 8-well glass slides (Millipore, PEZGS0816) at $5 \times 10^4$ cells per well and cultured in supplemented MV2 medium for 24 h. The medium was then removed, and the cells were incubated under different experimental conditions (± different peptides and ± 50 μM of MG in supplemented MV2 medium), as described above. For testing if Pep11-AGEs increase RAGE expression, cells were treated 250 μM of Pep11-AGEs or 100 μg/ml of HSA-AGEs as a positive control. After 24 h, the cells were fixed in 4% PFA for 15 min at room temperature, permeabilized with 0.1% Triton X-100 for 10 min at room temperature, and then blocked using 10% normal goat serum (BioLynx, Cat#VECTS1000) for 1 h at room temperature and then incubated with primary antibodies overnight at 4 °C in the dark. The primary antibody used for immunostaining was Anti-RAGE (1:200, Abcam, Cat#ab30381). After primary antibody incubation, slides were washed with PBS several times and then incubated with AF568 anti-rabbit secondary antibodies (ThermoFisher, Cat#A-11036 at 1:500 dilution) at room temperature for 1 h in the dark. Nuclei were stained with DAPI (1:1000) and then slides were washed and mounted with fluorescence mounting medium (Dako, Cat# S3023). The mean fluorescent intensity for RAGE in images taken for at least 3 random fields-of-view for each well was calculated by ImageJ2 software.

**Western blot**

HCMECs were seeded into 6-well plates (5 x $10^5$ cells/well) and maintained in supplemented MV2 medium until they reached around 90% confluency. The medium was then removed, and the cells were incubated under different experimental conditions (± different peptides and ± 50 μM of MG in supplemented MV2 medium), as described above. After 24 h, the media was removed, and the cells were washed with ice-cold PBS. Then, ice-cold RIPA lysis buffer containing protease/phosphatase inhibitor cocktail (Roche, Cat# 04693159001) was added to the wells. Wells were scraped using a cold plastic cell scraper to detach any adherent cell contents, and the cell lysates were then transferred into microcentrifuge tubes. The tubes were agitated for 30 min at 4 °C, and following this, the contents were centrifuged at 14,000 g for 15 min at 4 °C. The total protein concentrations were then measured using a Pierce™ BCA Protein Assay Kit (Fisher Scientific, Cat#PI23225) according to the manufacturer's protocol. Samples were heated at 95 °C for 5 min, and equal amounts of protein (20 μg) were loaded onto a 4-10% SDS gel and run at 100 V for 90 min in running buffer. Proteins were transferred to PVDF membranes (Bio-Rad Laboratories) at 100 V for 90 min in transfer buffer. Membranes were blocked for 1 h at room temperature with 5% skim milk in Tris-buffered saline-Tween20 (TBS-T). The immunoblots were probed with anti-MG derived AGE Antibody (Novus Biologicals, Mouse, Cat#NBP2-62810 at 1:500 dilution), anti-Glo1 (Novus Biologicals, Rabbit, Cat#NBP1-31466 at 1:1000 dilution), and anti-α-tubulin (Cell Signaling, Rabbit, Cat#2125 at 1:1000 dilution) primary antibodies overnight. After washing with TBS-T several times, membranes were incubated with anti-rabbit (Novus Biologicals, HRP, Cat#N7185 at 1:10000 dilution) or anti-mouse (Abcam, HRP, Cat#ab205719 at 1:10000 dilution) secondary antibodies for 1 h at RT. Protein bands were visualized using the Chemidoc Imaging System. Bands were quantified using densitometry analysis in ImageJ2 software, and intensities of the bands were normalized to α-tubulin. Briefly, a rectangular box was drawn around the selected protein bands of interest to perform band densitometry. The same-sized rectangular boxes were used to measure all bands.

**Protocol for Pep11 and HSA glycation products**

Recombinant human serum albumin (HSA) was glycated according the method of Croes et al.,[64] with minor modifications. Briefly, HSA (30 mg/mL) was incubated in 100 mM phosphate buffer (pH 7.4) ± 50 μM of MG at 37 °C for 24 h. After glycation, the protein and its corresponding control were washed 5 times with 50-kDa Amicon centrifugal filters to remove excess MG. In each

washing step, 500 µL of the sample was brought to a final volume of 4 mL with buffer. Samples were stored at -20 °C until use. The presence of MG-H1 was confirmed by dot blot (see below). For evaluating the MG-modified Pep11 products, 250 µM Pep11 was incubated in 100 mM phosphate buffer (pH 7.4) ± 50 µM of MG at 37 °C for 24 h. The glycated Pep11 products that were formed were then analyzed by HPLC-MS, as described above.

**Dot blot**

A nitrocellulose membrane was used for dot blotting. A total of 15 µL of the sample was spotted onto the membrane, yielding a final concentration of 30 µg. The membrane was then blocked with 3% BSA in TBS-T (0.1% Tween-20) for 1 h at RT. After blocking, the membrane was washed 3 × 5 min with TBS-T, followed by incubation with anti-MG-H1 antibody (Novus Biologicals, Mouse, Cat#NBP2-62810 at 1:1000 dilution) in 3% BSA in TBS-T at 4°C overnight. The next day, the membrane was washed 3 × 5 min with TBS-T, then incubated with anti-mouse secondary antibody (Abcam, HRP, Cat#ab205719) at 1:10000 dilution for 1 h at RT. Proteins were visualized using the Chemidoc Imaging System.

**Statistics**

Statistical analysis and fitting were performed using GraphPad Prism 10.3.1 (GraphPad, San Diego, CA). Statistical differences for the results in Figures 2 and 3 were determined using one-way ANOVA followed by Tukey's test. (*$p < 0.05$; **$p < 0.01$; ****$p < 0.0001$). Statistical differences for the results in Figures 5 and 6 were determined using one-way ANOVA followed by the Bonferroni test. (*$p < 0.05$; **$p < 0.01$; ****$p < 0.0001$).

## Data availability

All data are available in the main article and supplementary information and are openly available in FigShare at https://figshare.com/s/b8c4421feed97495ad43.

## References


1. Trujillo, M. N. & Galligan, J. J. Reconsidering the role of protein glycation in disease. *Nat. Chem. Biol.* **19**, 922-927 (2023).
2. Uceda, A. B., Mariño, L., Casasnovas, R. & Adrover, M. An overview on glycation: molecular mechanisms, impact on proteins, pathogenesis, and inhibition. *Biophys. Rev.* **16**, 189-218 (2024).

3. Prasad, C., Davis, K. E., Imrhan, V., Juma, S. & Vijayagopal, P. Advanced glycation end products and risks for chronic diseases: Intervening through lifestyle modification. *Am. J. Lifestyle Med.* **13**, 384-404 (2019).
4. Khalid, M., Petroianu, G. & Adem, A. Advanced glycation end products and diabetes mellitus: Mechanisms and perspectives. *Biomolecules* **12**, 542 (2022).
5. Mengstie, M.A. et al. Endogenous advanced glycation end products in the pathogenesis of chronic diabetic complications. *Front. Mol. Biosci.* **9**, 1002710 (2022).
6. Li, J., Liu, D., Sun, L., Lu, Y. & Zhang, Z. Advanced glycation end products and neurodegenerative diseases: Mechanisms and perspective. *J. Neurol. Sci.* **317**, 1-5 (2012).
7. Chegão, A. et al. Glycation modulates glutamatergic signaling and exacerbates Parkinson's disease-like phenotypes. *NPJ Parkinsons Dis.* **8**, 51 (2022).
8. Mulder, D. J. et al. Skin autofluorescence is elevated in acute myocardial infarction and is associated with the one-year incidence of major adverse cardiac events. *Neth. Heart J.* **17**, 162-168 (2009).
9. Hartog, J. W. et al. Clinical and prognostic value of advanced glycation end-products in chronic heart failure. *Eur. Heart J.* **28**, 2879-2885 (2007).
10. Lo, T., Westwood, M. E., McLellan, A. C., Selwood, T. & Thornalley, P. J. Binding and modification of proteins by methylglyoxal under physiological conditions. A kinetic and mechanistic study with N alpha-acetylarginine, N alpha-acetylcysteine, and N alpha-acetyllysine, and bovine serum albumin. *J. Biol. Chem.* **269**, 32299-32305 (1994).
11. Alhujaily, M. Molecular assessment of methylglyoxal-induced toxicity and therapeutic approaches in various diseases: exploring the interplay with the glyoxalase system. *Life* **14**, 263 (2024).
12. Berdowska, I., Matusiewicz, M. & Fecka, I. Methylglyoxal in cardiometabolic disorders: routes leading to pathology counterbalanced by treatment strategies. *Molecules* **28**, 7742 (2023).
13. Lai, S. W. T., Lopez Gonzalez, E. D. J., Zoukari, T., Ki, P. & Shuck, S. C. Methylglyoxal and its adducts: Induction, repair, and association with disease. *Chem. Res. Toxicol.* **35**, 1720-1746 (2022).
14. Rabbani, N. & Thornalley, P. J. Methylglyoxal, glyoxalase 1 and the dicarbonyl proteome. *Amino Acids* **42**, 1133-1142 (2012).
15. Rabbani, N., Xue, M. & Thornalley, P. J. Methylglyoxal-induced dicarbonyl stress in aging and disease: first steps towards glyoxalase 1-based treatments. *Clin. Sci.* **130**, 1677-1696 (2016).
16. Yao, D. & Brownlee, M. Hyperglycemia-induced reactive oxygen species increase expression of the receptor for advanced glycation end products (RAGE) and RAGE ligands. *Diabetes* **59**, 249-255 (2010).
17. Ahmed, N. et al. Methylglyoxal-derived hydroimidazolone advanced glycation end-products of human lens proteins. *Invest. Ophthalmol. Vis. Sci.* **44**, 5287-5292 (2003).
18. Ceradini, D. J. et al. Decreasing intracellular superoxide corrects defective ischemia-induced new vessel formation in diabetic mice. *J. Biol. Chem.* **283**, 10930-10938 (2008).
19. Akhand, A. A. et al. Glyoxal and methylglyoxal trigger distinct signals for map family kinases and caspase activation in human endothelial cells. *Free Radic. Biol. Med.* **31**, 20-30 (2001).
20. Lee, J. H. et al. Molecular mechanisms of methylglyoxal-induced aortic endothelial dysfunction in human vascular endothelial cells. *Cell Death Dis.* **11**, 403 (2020).

21. Vulesevic, B. et al. Methylglyoxal-induced endothelial cell loss and inflammation contribute to the development of diabetic cardiomyopathy. *Diabetes* **65**, 1699-1713 (2016).
22. Zhou, M. et al. Activation and modulation of the AGEs-RAGE axis: Implications for inflammatory pathologies and therapeutic interventions – A review. *Pharmacol. Res.* **206**, 107282 (2024).
23. Baig, M. H. et al. Methylglyoxal and advanced glycation end products: Insight of the regulatory machinery affecting the myogenic program and of its modulation by natural compounds. *Sci. Rep.* **7**, 5916 (2017).
24. Goldin, A., Beckman, J. A., Schmidt, A. M. & Creager, M. A. Advanced glycation end products: sparking the development of diabetic vascular injury. *Circulation* **114**, 597-605 (2006).
25. Nowotny, K. et al. Oxidants produced by methylglyoxal-modified collagen trigger ER stress and apoptosis in skin fibroblasts. *Free Radic. Biol. Med.* **120**, 102-113 (2018).
26. McLaughlin, S. et al. Recombinant human collagen hydrogel rapidly reduces methylglyoxal adducts within cardiomyocytes and improves borderzone contractility after myocardial infarction in mice. *Adv. Funct. Mater.* **32**, 2204076 (2022).
27. Guo, X., Ileri, R., Ruel, M., Alarcon, E. I. & Suuronen, E. J. Being a target for glycation by methylglyoxal contributes to therapeutic efficacy of injectable collagen hydrogels post-myocardial infarction. *Gels* **12**, 18 (2026).
28. Blackburn, N. J. R. et al. Methylglyoxal-derived advanced glycation end products contribute to negative cardiac remodeling and dysfunction post-myocardial infarction. *Basic Res. Cardiol.* **112**, 1-14 (2017).
29. Katiyar, N. K., Goel, G., Hawi, S. & Goel, S. Nature-inspired materials: Emerging trends and prospects. *NPG Asia Mater.* **13**, 56 (2021).
30. Wang, L. et al. Therapeutic peptides: current applications and future directions. *Signal Transduct. Targete. Ther.* **7**, 48 (2022).
31. Xiao, W. et al. Advance in peptide-based drug development: delivery platforms, therapeutics and vaccines. *Signal Transduct. Targete. Ther.* **10**, 74 (2025).
32. Sasaki, N. A. et al. N-Terminal 2,3-diaminopropionic acid (Dap) peptides as efficient methylglyoxal scavengers to inhibit advanced glycation endproduct (AGE) formation. *Bioorg. Med. Chem.* **17**, 2310-2320 (2009).
33. Brings, S. et al. A scavenger peptide prevents methylglyoxal induced pain in mice. *Biochim. Biophys. Acta Mol. Basis Dis.* **1863**, 654-662 (2017).
34. Diao, L. & Meibohm, B. Pharmacokinetics and pharmacokinetic–pharmacodynamic correlations of therapeutic peptides. *Clin. Pharmacokinet.* **52**, 855-868 (2013).
35. Conticello, V. P. Peptide-based nanomaterials: Building back better & beyond. *Curr. Opin. Solid State Mater. Sci.* **27**, 101066 (2023).
36. Lee, N. R., Bowerman, C. J. & Nilsson, B. L. Effects of varied sequence pattern on the self-assembly of amphipathic peptides. *Biomacromolecules* **14**, 3267-3277 (2013).
37. Ulijn, R. V. & Smith, A. M. Designing peptide based nanomaterials. *Chem. Soc. Rev.* **37**, 664-675 (2008).
38. Ligorio, C. & Mata, A. Synthetic extracellular matrices with function-encoding peptides. *Nat. Rev. Bioeng.* **1**, 518-536 (2023).
39. Kumar, V. A. et al. A nanostructured synthetic collagen mimic for hemostasis. *Biomacromolecules* **15**, 1484-1490 (2014).

40. Uysal, O. et al. Collagen peptide presenting nanofibrous scaffold for intervertebral disc regeneration. *ACS Appl. Bio Mater.* **2**, 1686-1695 (2019).
41. Ross, A. et al. Multipurpose on-the-spot peptide-Based hydrogels for skin, cornea, and heart repair. *Adv. Funct. Mater.* **34**, 2402564 (2024).
42. Ross, A. et al. Mechanically stable and tunable photoactivated peptide-based hydrogels for soft tissue adhesion. *Adv. Funct. Mater* **36**, e29084 (2026).
43. McEwen, J. M., Fraser, S., Guir, A. L. S., Dave, J. & Scheck, R. A. Synergistic sequence contributions bias glycation outcomes. *Nat. Commun.* **12**, 3316 (2021).
44. Lyu, C. et al. Advanced glycation end-products as mediators of the aberrant crosslinking of extracellular matrix in scarred liver tissue. *Nat. Biomed. Eng.* **7**, 1437-1454 (2023).
45. Wild, R., Ooi, L., Srikanth, V. & Münch, G. A quick, convenient and economical method for the reliable determination of methylglyoxal in millimolar concentrations: the N-acetyl-l-cysteine assay. *Anal. Bioanal. Chem.* **403**, 2577-2581 (2012).
46. Rabbani, N. & Thornalley, P. J. Measurement of methylglyoxal by stable isotopic dilution analysis LC-MS/MS with corroborative prediction in physiological samples. *Nat. Protoc.* **9**, 1969-1979 (2014).
47. Van Lancker, F., Adams, A. & De Kimpe, N. Impact of the N-terminal amino acid on the formation of pyrazines from peptides in Maillard model systems. *J. Agric. Food Chem.* **60**, 4697-4708 (2012).
48. Bunn, H. F., Haney, D. N., Gabbay, K. H. & Gallop, P. M. Further identification of the nature and linkage of the carbohydrate in hemoglobin A1c. *Biochem. Biophys. Res. Commun.* **67**, 103-109 (1975).
49. Martin, M. S., Jacob-Dolan, J. W., Pham, V. T. T., Sjoblom, N. M. & Scheck, R. A. The chemical language of protein glycation. *Nat. Chem. Biol.* **21**, 324-336 (2024).
50. Kingkeohoi, S. & Chaplen, F. W. R. Analysis of methylglyoxal metabolism in CHO cells grown in culture. *Cytotechnol.* **48**, 1-13 (2005).
51. Avilés-Moreno, J. R., Berden, G., Oomens, J. & Martínez-Haya, B. Insights into the recognition of phosphate groups by peptidic arginine from action spectroscopy and quantum chemical computations. *J. Phys. Chem. B* **123**, 7528-7535 (2019).
52. Mamsa, S. S. A. & Meloni, B. P. Arginine and arginine-rich peptides as modulators of protein aggregation and cytotoxicity associated with Alzheimer's disease. *Front. Mol. Neurosci.* **14**, 759729 (2021).
53. Sena, C. M. et al. Methylglyoxal promotes oxidative stress and endothelial dysfunction. *Pharmacol. Res.* **65**, 497-506 (2012).
54. Pucci, M. et al. Methylglyoxal affects cognitive behaviour and modulates RAGE and Presenilin-1 expression in hippocampus of aged mice. *Food Chem. Toxicol.* **158**, 112608 (2021).
55. Tanaka, N. et al. The receptor for advanced glycation end products is induced by the glycation products themselves and tumor necrosis factor-α through nuclear factor-κB, and by 17β-estradiol through Sp-1 in human vascular endothelial cells. *J. Biol. Chem.* **275**, 25781-25790 (2000).
56. Kim, G., Yoo, H. J., Yoo, M. K., Choi, J. H., & Lee, K. W. Methylglyoxal-derived hydroimidazolone-1/RAGE axis induces renal oxidative stress and renal fibrosis in vitro and in vivo. *Toxicol*. **507**, 153887 (2024).

57. Tin Pham, V. T., Datta, S., Sterling, A. C., Hansel, S. M. & Scheck, R. A. A chemical mechanistic path leads the way to cellular argpyrimidine. *J. Am. Chem. Soc.* **147**, 38055-38068 (2025).
58. Jacob-Dolan, J. W., Sterling, A. C., Brutus, M. E., Hansel, S. M. & Scheck, R. A. Discovery of glycation-derived cross-links at arginine. *J. Am. Chem. Soc.* **148**, 6840-6849 (2026).
59. Merrifield, R. B. Solid phase peptide synthesis. I. The Synthesis of a tetrapeptide. *J. Am. Chem. Soc.* **85**, 2149-2154 (1963).
60. Essmann, U. et al. A smooth particle mesh Ewald method. *J. Chem. Phys.* **103**, 8577-8593 (1995).
61. York, D. M., Darden, T. A. & Pedersen, L. G. The effect of long-range electrostatic interactions in simulations of macromolecular crystals: A comparison of the Ewald and truncated list methods. *J. Chem. Phys.* **99**, 8345-8348 (1993).
62. Bussi, G., Donadio, D. & Parrinello, M. Canonical sampling through velocity rescaling. *J. Chem. Phys.* **126**, 014101 (2007).
63. Berendsen, H. J. C., Postma, J. P. M., van Gunsteren, W. F., DiNola, A. & Haak, J. R. Molecular dynamics with coupling to an external bath. *J. Chem. Phys.* **81**, 3684-3690 (1984).
64. Croes, C.-A. C. C. et al. Diabetic glycation of human serum albumin affects its immunogenicity. *Biomolecules* **14**, 1492 (2024).

## Acknowledgments

Funding was provided by an operating grant from the Canadian Institutes of Health Research (PJT-183748; to E.J.S), a discovery grant from the Natural Sciences and Engineering Research Council (NSERC; RGPIN-2023-03813; to E.I.A.), and by a University of Ottawa Research Chair to E.I.A. E.I.A. and E.J.S. also thank NSERC's support of the INTBIOTECH-CREATE program. S.D.G.S. thanks the University of Ottawa Heart Institute (UOHI) Foundation and the University of Ottawa Cardiac Endowment Fund for a strategic research Postdoctoral Fellowship. J.D.F.A. thanks the University of Ottawa Heart Institute and the MITACS Elevate Thematic Postdoctoral Fellowship Program. R.I. was supported by a strategic scholarship from the University of Ottawa Cardiac Endowment Fund and a Study Abroad PhD Programme scholarship from the Turkish Ministry of National Education (YLSY). Peptides were synthesized in the Advanced Peptide Core Facility at the University of Ottawa Heart Institute, which is funded by an NSERC-RTI award and the Canadian Foundation for Innovation John R. Evans Leaders Fund (to E.I.A.). The schematics in Figures 1 and 3 were created using BioRender. The authors would like to thank Dr. Marcelo Muñoz and Ahmed El-Hamad for technical assistance.

## Competing interests

S.D.G.S., J.D.F.A., R.I., M.G., J.H.J., E.I.A., E.J.S. are listed as inventors in a patent application for the peptide technology presented herein. Patent applicant: Ottawa Heart Institute Research Corporation, 40 Ruskin Street H2406 Ottawa, Ontario K1Y 4W7, Canada. Name of inventors: Sergio D. Garcia Schejtman, Juan D. Figueroa Alegria, Ramis Ileri, Micaela Giannetti, Jessica Hernandez Juarez, Emilio I. Alarcon, Erik J. Suuronen. Application number: US 63/935,135. Status of the application: filed on 12/09/2025. The specific aspect of manuscript covered in the patent application: Composition of matter for the collagen-like peptides, and the use of the collagen-like peptides as a methylglyoxal-trapping therapeutic agent.

## Author contributions

† S.D.G.S., J.D.F.A. and R.I. contributed equally to this work. E.J.S., E.I.A., S.D.G.S., J.D.F.A., R.I.: Study design. S.D.G.S., J.D.F.A., J.H.J., B.L.: Peptide design, synthesis, characterization, and testing. E.J.S., R.I.: In vitro assay design and optimization. M.G.: Molecular simulations and script optimization. E.J.S., E.I.A., S.D.G.S., J.D.F.A., R.I.: Data discussion and analyses. E.J.S. and E.I.A. provided supervision. S.D.G.S., J.D.F.A., R.I., E.I.A. and E.J.S. wrote the manuscript with input from all authors. All authors have reviewed and approved the final version of the manuscript.

## Supplementary Files

This is a list of supplementary files associated with this preprint. Click to download.

- NatCommun2026GarciaSchejtmanetalSupportinginformation.pdf